

# Oxygen doping-induced photogeneration loss in P3HT:PCBM solar cells

Antonio Guerrero<sup>1\*</sup>, Pablo P. Boix<sup>1</sup>, Luís F. Marchesi<sup>1,2</sup>, Teresa Ripolles-Sanchis<sup>1</sup>, Ernesto C. Pereira<sup>2</sup>, and Germà Garcia-Belmonte<sup>1\*</sup>

*1 Photovoltaic and Optoelectronic Devices Group, Departament de Física, Universitat Jaume I, ES-12071 Castelló, Spain*

*2 Laboratório Interdisciplinar de Electroquímica e Cerâmica (LIEC), Universidade Federal de São Carlos, São Carlos, Brazil*

## Abstract

This work investigates the loss in performance induced by molecular oxygen in bulk heterojunction solar cells. We observe that upon exposure to molecular oxygen both formation of P3HT<sup>+</sup>:O<sub>2</sub><sup>-</sup> complex, and metal oxidation at the interface between the active layer and metallic contact occur. These two different effects were separately investigated by using NOBF<sub>4</sub> as oxidant. Our procedure has allowed studying *p*-doping of the active layer independently from contact degradation. A loss in photocurrent is associated with formation of P3HT<sup>+</sup>:O<sub>2</sub><sup>-</sup> complex which reduces the concentration of neutral P3HT present in the film in accordance with absorption and external quantum efficiency spectra. This complex is regarded as a source of a pathway of reversible degradation. Capacitance-voltage measurements allow for an accurate extraction of *p*-doping levels of the active layer produced by the presence of charged, O<sub>2</sub><sup>-</sup> species. In addition, one of the irreversible degradation pathways is identified to be oxidation of the metallic contact to form CaO. This oxide forms a thin dipole layer producing a voltage drop across the active layer/Ca interface, which has a direct impact in the open circuit voltage and fill factor.

*Keywords:* Organic photovoltaics, oxygen doping, capacitance, degradation.

\*Corresponding authors: A. Guerrero, e-mail: [aguerrer@uji.es](mailto:aguerrer@uji.es), tel.: +34 964 387463, fax: +34 964 729218 and G. Garcia-Belmonte, e-mail: [garciag@uji.es](mailto:garciag@uji.es), tel.: +34 964 387548, fax: +34 964 729218

## 1. Introduction.

Organic solar cells have attracted much attention over the last decade, and currently power conversion efficiencies over 8% have been reported [1]. In order to obtain further improvements in long-term solar cell performance a detailed understanding of the device stability and degradation mechanisms are required [2]. Known degradation mechanisms include: diffusion of molecular oxygen and water into the device [3], degradation of interfaces [4], degradation of the active material [5], interlayer and electrode diffusion [6] or electrode reaction with the organic materials [7]. In regular architecture solar cells prepared in ambient conditions oxygen has always been regarded as a source of cell performance losses [8]. In terms of chemical modifications oxygen plays an important role as it is responsible for chemical degradation pathways in the dark and, more rapidly, in combination with light [4]. Indeed, degradation of systems comprising P3HT [9] and C<sub>60</sub> [10, 11] induced by oxygen has been reported decreasing carrier mobilities and enhancing trap densities. Additionally, the effect of oxygen has normally been related to degradation of the metallic aluminium or calcium contact to form oxides in a regular configuration [12].

There is some controversy on the role of oxygen as a degradation source. On the one hand, P3HT has been reported to form a complex with oxygen [13, 14]. However, in the solid state even at high concentrations of singlet oxygen the solid film has been reported to remain unaltered [15]. Thus, degradation of the film appears to take place through a radical mechanism which requires to overcome an activation energy [16]. Interestingly, recent studies on degradation pathways induced by oxygen of semipermeable bulk heterojunction cells have identified components of both reversible and irreversible degradation [17]. In that work reversible degradation of the cells in the presence of oxygen resulted mainly in the reduction of short circuit current, while the loss in light absorption was negligible. However, we experimentally observe by submitting the cells to a controlled oxygen exposure that a simultaneous decrease in both photocurrent and absorption exists, in agreement with the increase of *p*-doping level extracted from capacitance-voltage analysis. A direct connection is then established between an oxygen-related degradation route and cell performance parameters.

The specific goal of our work is to understand the effects of oxygen on the active layer blend (P3HT:PCBM) and contact in bulk heterojunction cells of regular configuration. Since the metallic contact oxidation may occur simultaneously with the

blend degradation, we follow a robust fabrication method in air and treat the samples with different oxidant sources prior to cathode deposition. The cell preparation procedure allows us to separate degradation contributions originated at the device bulk from those occurring at the outer interface. Recently, regular organic solar cells fabricated in air have been reported to provide similar performances to those of devices produced under a nitrogen atmosphere [18]. This fact would suggest that the origin of device degradation is not induced during device fabrication, but because of oxygen or water diffusion. Hence chemical degradation only begins to be evident after the cathode has been deposited and the cell has been completed. The present work demonstrates the formation of a P3HT complex with oxygen (highly reversible), which is related to the photocurrent decrease and monitored through capacitance-voltage measurements. Additionally, generation of metallic oxide layers as CaO at the cathode contact interface (completely irreversible) is observed.

## **2. Experimental**

### *2.1. Samples preparation and oxygen exposure.*

In this work we follow photovoltaic cells fabrication process carried out in air [18]. A detailed description of the experimental conditions can be found in the Appendix A. We briefly describe here the process for our control cell (cell 1, Table I). First, we prepared all the mixed P3HT:PCBM solutions in a glovebox filled with a nitrogen atmosphere using dry o-dichlorobenzene (ODCB). Films are spin cast in air and the active layer was “solvent annealed” in a Petri dish for 2 hours. At this point cells were transferred to the glovebox to undergo a thermal annealing treatment to provide “oxygen free” active layer. For our photovoltaic cells we found optimum cell efficiencies when heated at 150°C for 10 min and these conditions were used for all devices described in this work. Cell 1 was kept in the glovebox throughout the time from the thermal treatment to device encapsulation [19]. Note that device encapsulated is required to avoid oxygen contamination from the environment. The polymer solar cells were fabricated with a standard sandwich structure of ITO/PEDOT:PSS/P3HT:PCBM/Ca/Ag.

As reported by Mattis et al. [20] the annealing temperature required to promote oxygen desorption needs to be above 120°C. Thus, we did not carry out a second thermal treatment after contact evaporation which usually improves cell performance. For oxygen doped samples a second annealing treatment would induce oxygen desorption and in that case we would not be able to measure the intentionally introduced

oxygen doping (see Table I). Hence only one annealing step is necessary to obtain an adequate morphology and to provide effective oxygen desorption in P3HT prior to cathode deposition. As a result optimum efficiencies were found for devices with an active layer thickness of 400 nm. This is considerably higher than values usually reported in P3HT:PCBM photovoltaic cells (ca. 150-250 nm). All the cells presented in this study followed this processing, introduction of oxygen or a different oxidant into the system was carried out as explained below.

Oxygen treatment is implemented at different stages. For sample 2 traces of water that may be present in the films (i.e. PEDOT:PSS is highly hygroscopic) are carefully eliminated in the glovebox after the “solvent cure” step. The substrate was placed under vacuum and was heated to 50 °C for 1 hour. Further traces of water were eliminated by introducing the sample in a high vacuum chamber in the glovebox at a pressure of  $1 \times 10^{-6}$  mbar over night. After this exhaustive elimination of water the film was annealed to obtain an adequate morphology. The sample was placed in a sealed portable chamber with no-return valves to provide a flow of dry synthetic compressed air (ca. nitrogen 80 % and oxygen 20 %) during 2 hours. Cells 3 and 4 were treated with dry synthetic compressed air after annealing in the same set up without exhaustively removing traces of water. Finally, sample 5 was doped with molecular oxygen by saturation of the P3HT:PCBM solution with dry oxygen before spin coating.

In a second set of experiments  $\text{NOBF}_4$  was used as oxidant. For cells 6 to 8 this oxidant is introduced in the system before spin cast the active layer. P3HT reacts with  $\text{NOBF}_4$  to provide a very dark solution and a solid. The reaction product was added to the P3HT:PCBM blend to provide the  $\text{NOBF}_4$  concentration described in Table I ( $\sim 1 \times 10^{-6}$  M). On the other hand, sample 9 was treated with  $\text{NOBF}_4$  in acetonitrile directly after spin coating the active layer at considerably higher concentration ( $1 \times 10^{-2}$  M).

### **3. Results**

#### *3.1. Current density-voltage curves*

Figure 1 shows the current density-voltage curves for all analyzed samples and Table II summarises their photovoltaic parameters. Optimum efficiencies were found for devices with an active layer thickness of 400 nm. Considering this large thickness, the reference sample (cell 1) shows a relatively high efficiency (2.8 %) with high fill factor (FF) and open circuit voltage ( $V_{oc}$ ). However, the short circuit current ( $J_{sc}$ ) is

considerably lower than that obtained for thinner cells which are reported to provide  $>10 \text{ mA/cm}^2$  [21]. Cells doped with oxygen show decreased performance with increasing oxygen exposure. Cell 2 that was meticulously dried and treated with dry synthetic air for 2 h shows very similar results to those obtained for the reference cell. Cell 3 (1 h oxygen treatment and no additional drying step) shows similar  $V_{oc}$  to that of the reference cell and cell 2. However, the  $J_{sc}$  was slightly reduced and the FF decreases from 58% for cell 1 to 45% for cell 3. An additional hour of exposure to oxygen on cell 4 further decreased the photocurrent and the photovoltage began to be affected. Modifying the exposure method to oxygen for Cell 5 provided very similar device parameters to cell 4 with slightly reduced  $V_{oc}$  and increased FF.

A second set of devices used  $\text{NOBF}_4$  as oxidizing agent. We followed a fabrication process analogous to that employed for cell 5 but using  $\text{NOBF}_4$  in solution instead of dry synthetic air. The current density-voltage curves for cells doped with  $\text{NOBF}_4$  are shown in Fig. 1 (right). As occurring for oxygen doping, an increment in solution concentration containing  $\text{NOBF}_4$  decreases  $J_{sc}$  and  $V_{oc}$  gradually. However, in contrast to samples doped with oxygen where the FF is reduced significantly devices doped with  $\text{NOBF}_4$  only show a slight decrease for sample 8. Processing conditions for sample 9 involved high concentrations of  $\text{NOBF}_4$ . It should be noticed that in order to obtain a working device with conditions for cell 9 a different metallic contact was used (LiF/Al/Ag). Interestingly, the replacement of the metallic contact both helps to recover device performance (from 0.006 % to 1.4 %). A detailed discussion can be found in the Appendix A.

### *3.2. Optical properties of materials, films and relation with EQE*

In order to understand whether the reaction of P3HT:PCBM blend with molecular oxygen give rise to similar polymer oxidation than those obtained with  $\text{NOBF}_4$  we carried out characterization by absorption measurements in solution. First a solution containing PCBM in ODCB was either treated with molecular oxygen or  $\text{NOBF}_4$  at room temperature and no spectroscopic difference was observed after 24 h. Then, a solution containing P3HT in ODCB was treated with dry oxygen for 30 seconds at room temperature. The spectrum is shown in Figure 2 and clearly shows that the creation of new species reduces the intensity of the absorption peak of P3HT as this polymer takes part on complex formation. A new absorption band is generated towards the infrared with a maximum peak at 810 nm, which is attributed to polaronic transitions [22]. This

new band is then assigned here to the complex  $\text{P3HT}^+:\text{O}_2^-$  formed by reaction of P3HT and oxygen (Scheme 1a) [13]. Additionally, the reaction product between P3HT and  $\text{NOBF}_4$  was also characterised by absorption measurements. Both reactions of P3HT with either  $\text{O}_2$  or  $\text{NOBF}_4$  produce similar absorption response in solution using ODCB as solvent. Chemically the main difference between both oxidants is that in this last case we expect the reaction to be irreversible as NO gas is evolved (Scheme 1b) being the counterion  $\text{BF}_4^-$  for the second oxidant.

In order to analyze the effect of oxygen doping on the photocurrent we measure the steady-state absorption of films processed under the same conditions of the referred cells (without the cathode contact). Films 1-3 exhibit similar absorption spectra in terms of intensities and absorption onsets (Figure 3a, left). These findings are in perfect agreement with those discussed by Seeman in which they did not observe any change in the absorption intensity with exposure to dry synthetic air [17]. However, films 4 and 5 show reduced absorption intensity for P3HT and, interestingly, the intensity in the absorption in the 650-700 nm region is slightly altered. Similarly, films doped with  $\text{NOBF}_4$  confirmed the same trend observed for oxygen doping. Increasing the concentration of  $\text{NOBF}_4$  led to decreased intensity of the P3HT absorption and increased absorption towards long wavelengths.

EQE measurements of the corresponding cells were also performed. A correlation for all cells under study between intensities obtained from absorption spectra and EQE is clear: Reduced absorption led to reduced charge collection in the same proportion. Interestingly, none of the cells show increase charge collection in the 700-800 nm region. This is especially noticeable for cell 9 using high  $\text{NOBF}_4$  concentration that even showing a clear band in the red region does not contribute to the extracted charges as inferred from EQE measurements.

### 3.3. Capacitance-voltage analysis.

Analysis of capacitance-voltage ( $C-V$ ) measurements has become a standard technique to extract relevant material parameters. In previous work, we showed that for organic photovoltaics information extracted from  $C-V$  measurements are related to the  $p$ -doping level resulting from acceptor defect states within the polymer band gap [23]. Standard P3HT:PCBM solar cells showed Mott–Schottky characteristics, exhibiting full depletion at reverse bias and a linear relationship at low forward bias (0.0–0.5 V) [23]. The density of fully ionized defect states ( $p$ -doping level)  $n$  was derived from the slope

by means of the Mott–Schottky relation

$$C^{-2} = \frac{2(V_{fb} - V)}{A^2 q \varepsilon \varepsilon_0 n} \quad (1)$$

Where  $A$  corresponds to the device active surface,  $\varepsilon$  is the relative dielectric constant of the blend,  $\varepsilon_0$  the permittivity of the vacuum, and  $n$  the total concentration of acceptor impurities (intrinsic defects with additional charged immobile  $O_2^-$  or  $BF_4^-$  counterions). It is assumed that the defect density explored from capacitance corresponds to those defects able to follow measuring frequency. Thus, by analyzing the curve  $C^{-2}(V)$  one can extract  $V_{fb}$  from the intercept and the total concentration of acceptor impurities from the slope ( $n$ ). The intercept of this straight line with the real axis is related to the flat-band potential, which corresponds to the energy offset between the hole Fermi level and the cathode metal effective work function (see Fig. 4b) Recently, this technique has been used to monitor oxygen doping levels in polymer solar cells [17].

By analysis of the  $C$ - $V$  measurements we were able then to obtain accurate values for  $p$ -doping of the polymer. It is worth noting that  $C$ - $V$  Mott-Schottky analysis is only sensitive to the density of ionized impurity levels. A Mott-Schottky plot for our devices clearly shows different slopes for the samples exposed to oxygen under different experimental conditions (Appendix A). For clarification, it is important to note that the reported Mott-Schottky plots do not show full depletion at  $\sim 1$  V of reverse bias. An estimation of the geometric capacitance gives rise to a value of 7 nF/cm<sup>2</sup>. Taking into account that the capacitance values observed are higher than this and that depletion width are below 100 nm at -1 V we can conclude that full depletion has not been obtained for devices with high doping levels. On the other hand, device 1 shows a depletion width at -1 V of 350 nm which is close to the device thickness indicating that at this voltage the cell begins to be fully depleted, and explains why the  $C^{-2}(V)$  curve exhibits saturation as cells are reversely polarized (see Appendix A).

The results extracted from Mott-Schottky plots are summarized in Table I. The total concentration of acceptor impurities ( $n$ ) confirms the lowest doping level ( $0.9 \times 10^{16}$  cm<sup>-3</sup>) for the control sample 1. This minimum doping level corresponds to structural defects of the polymer, and to extrinsic impurities that are inherent to the processing and purity degree of chemicals used. Values for cells treated with oxygen range from 1.0 to  $1.5 \times 10^{16}$  molecules per cm<sup>3</sup>. Slightly higher values are obtained for cell 5 doped by oxygen saturation of the spin coating solution.

Alternatively, the doping density of samples doped with a stock solution of

P3HT<sup>+</sup>:BF<sub>4</sub><sup>-</sup> (Cells 6-8) are clearly higher than those obtained for oxygen. This supports that with NOBF<sub>4</sub> used as oxidant irreversible processes take place (oxidant desorption is not possible). Finally, cell 9 doped with a highly concentrated solution of NOBF<sub>4</sub> gives rise to the highest doping levels ( $10.8 \times 10^{16} \text{ cm}^{-3}$ ).

In addition to the doping levels,  $V_{fb}$  was calculated by analysis of the Mott-Schottky characteristics. A baseline flat-band voltage value of 467 mV was obtained for sample 1. This increased for cell 2, treated with oxygen, and followed with a gradual decrease for the subsequent samples. On the other hand, for samples treated with NOBF<sub>4</sub>, where no oxidation of the metallic contact is expected, (Cell 4-8) increasing doping concentrations of the oxidant increases  $V_{fb}$  from values of 456 to 507 mV. Sample 9 provides a low value of 390 mV. The observed trends will be explained in detail in the Discussion section.

## 4. Discussion

### 4.1 Correlation between photocurrent and doping level.

Our experimental methodology enabled us to treat the P3HT:PCBM layer with oxygen before contacting the cathode metal. As supported by absorption measurements in solution it appears that PCBM does not react with oxidants such as molecular oxygen or NOBF<sub>4</sub> in ODCB at room temperature. P3HT does react with molecular oxygen to form P3HT<sup>+</sup>:O<sub>2</sub><sup>-</sup> complexes. We consider such complex formation as a primary source of solar cell long-term degradation. A correlation is observed between the measured doping levels, absorption spectra of the films, EQE results and the photocurrent obtained for operating cells. Thus, cells 1-3 show similar film absorption and EQE spectra with a measured maximum current of  $\sim 8 \text{ mA/cm}^2$ . On the contrary, cell 4 and 5 exhibit reduced collection of charge carriers to provide a maximum current of  $\sim 7 \text{ mA/cm}^2$ . These results correlate with the obtained  $J_{sc}$ , and corroborate the relationship between oxygen doping and loss in photocurrent through reduction in absorption caused by lower concentration of neutral P3HT. The drop in  $V_{oc}$  is explained by a reduction in light absorbed, because less photogenerated carriers reduces the occupancy of polymer and fullerene electronic states then inhibiting the Fermi level splitting which is the ultimate origin of the photovoltage [24]. This type of performance loss is expected to be partially reversible through oxygen desorption via further annealing treatments.

For cells treated with molecular oxygen we observe that under most conditions the density of fully ionized acceptor impurities is increased with respect to those obtained



for the reference cell 1. Attempts to increase the doping levels from the oxygen-free sample 1 to the slightly doped sample 2 shows this slight effect (Table 1). It is interesting to note that cells 2 and 4 were both exposed to oxygen for 2 h, but the first meticulously dried. Whilst the totally dried cell exhibit similar doping levels then the reference cell 1, cell 4 shows slightly higher doping levels. By comparison of the performance characteristics of cell 3 and 4 it is clear that the reduced performance is due to additional exposure to oxygen and not to reaction with traces of water. Higher doping concentrations were obtained by using a molecular oxygen doping process in solution (cell 5) prior to the annealing step.

Oxidation of the metallic contact with oxygen or water present at the interface was nevertheless expected. Thus, in order to totally avoid generation of CaO and truly understand the effect of oxidants in the active layer we carried out further experiments with NOBF<sub>4</sub>. Such oxidant agent allows us to investigate active layer *p*-doping without the effect of calcium oxidation. As previously commented upon, P3HT does indeed react with both oxidants generating analogous reaction products. The main consequence of this is that the P3HT absorption band intensity decreases. This intensity reduction is also observed when film absorption measurements are carried out in the NOBF<sub>4</sub> treated samples (Figure 3a, right). Additionally, a slight increase in the intensity in the 650-700 nm region is also observed for samples 7-8 doped with NOBF<sub>4</sub>. This increase in intensity is assigned to generation of the complex P3HT<sup>+</sup>:BF<sub>4</sub><sup>-</sup> as supported by the spectra of cell 9 whereby the concentration of NOBF<sub>4</sub> was increased by a 10<sup>4</sup> factor during film preparation. Interestingly, the EQE and current density results obtained for completed doped cells clearly correlate with the film absorption measurements. Note that the newly generated species do not contribute to the collected charges.

The previous findings strongly indicate that the decrease in photocurrent density observed in the complete cells is primary caused by a decreasing in light absorption, and not by losses produced during carrier transport to the collecting electrodes. Because collection efficiency diminishes as oxidation level is raised, the observed simultaneous reduction in intensity of both absorption and EQE spectra should be related to a loss in photogeneration of mobile carriers. Additionally, the decrease in photovoltage can also be explained by that decrease in photogeneration as  $V_{oc}$  depends on the amount of light absorbed able to yield separated charge carriers.

As aforementioned *C-V* analysis provides direct information about the density of dopants that are actually ionized contributing to the conductivity (*p*-doping). Therefore

oxidant doping modifies the concentration of mobile hole carriers as new chemical species are created. The immobile  $O_2^-$  or  $BF_4^-$  counterions contribute to the formation of a hole depletion zone near the cathode contact (band bending) which was monitored by the  $C-V$  technique. As observed total concentration of acceptor impurities are qualitatively in agreement with the spectroscopic measurements and the decrease in photocurrent observed for the complete cells. Figure 4 illustrates this correlation including all cells studied. As observed an experimental relationship as  $J_{sc} \propto n^{-0.14}$  is found between photocurrent and doping level extracted from  $C-V$  analysis. However it is hard to understand how an increment of  $p$ -doping level within one order of magnitude (from  $\sim 10^{16} \text{ cm}^{-3}$  up to  $10^{17} \text{ cm}^{-3}$ ) is able to induce such large decrease in light absorption which gives rise to  $\sim 33\%$  reduction in photocurrent (from  $8.13 \text{ mA cm}^{-2}$  down to  $5.74 \text{ mA cm}^{-2}$ ). Oxidation levels as calculated from the  $C-V$  analysis are only in the range of 0.1-0.01% of polymer monomers taking part of the reactions drawn in Scheme 1. This apparent discrepancy can be solved by recalling that  $C-V$  analysis only monitors the density of fully ionized charge species (those participating in the modulation of the depletion zone). It is then necessary to distinguish between  $O_2^-$  (or  $BF_4^-$ ) counterion able to yield mobile hole carriers, from those that keep the hole attached forming the neutral complex  $P3HT^+:O_2^-$  (or  $P3HT^+:BF_4^-$ ). Therefore we remark that only a portion of the total oxidized polymer units contribute to increase the mobile hole concentration.

#### 4.2 Effect of the metal cathode oxidation

Regarding the variation in  $V_{fb}$  observed for cells doped with oxygen, Figure 4 shows different energy diagrams that explain the effect of increasing the  $p$ -doping concentration. An undoped semiconductor before contacting exhibits an energy diagram as that showed in Figure 4a. The difference in energy between the Fermi Level ( $E_F$ ) and the HOMO will be the same to the difference in energy between  $E_F$  and the LUMO. As the material is doped ( $p$ -type),  $E_F$  will shift approaching the HOMO of the polymer. The difference in energy between the HOMO and  $E_F$  will be smaller as we increase the concentration of  $p$ -dopants (Figure 4b and 4c). In addition, when the active layer is placed in contact with a metal,  $E_F$  and the effective workfunction of the metal equilibrates at the interface. This equilibration gives rise to the band bending (electrical field confinement) at the interface vicinity [23]. The flat band potential equals the energy offset between the hole Fermi level and the effective cathode work function. As

*p*-doping is increased the position of the Fermi level will shift towards low energies producing an increment in  $V_{fb}$ . This situation is clearly observed for samples treated with  $NOBF_4$  where no oxidation of the metallic contact has taken place. Thus,  $V_{fb}$  increases with increasing doping concentrations as the hole  $E_F$  approaches further the HOMO of the P3HT.

Evidences for CaO generation are found for samples treated with oxygen. For cells 2-5  $V_{fb}$  gradually decreases from values of 543 mV (sample 2) to 419 mV (sample 5). By comparison of cells 5 and cell 6 with similar doping levels, it is clear from the values obtained from  $V_{fb}$  that oxidation of calcium takes place faster for the sample containing molecular oxygen as dopant. This indicates that upon exposure to oxygen part of the molecular oxygen will produce  $P3HT^+ : O_2^-$  complexes, while other part will generate calcium oxide. Generation of CaO will then be responsible for a drop in  $V_{fb}$  as schematically depicted in Figure 4c and 4d [25]. This oxide accommodates part of the applied voltage during *C-V* measurement because of the formation of a dipole layer. Similar energy level shifts have been reported previously for organic/metal interfaces [26]. Thus, an increase in the oxygen exposure provides simultaneously P3HT *p*-doping increment and decrease in  $V_{fb}$ . It is important to note that generation of CaO has taken place to a very small degree as supported by a slightly increased series resistance observed for the sample doped with molecular oxygen (see Appendix A). Presence of CaO clearly has a negative impact in the FF which reduces from nearly 60 to 45, contrary to the case of using  $NOBF_4$  as dopant. It is interesting to note is that cells doped with  $NOBF_4$  (samples 6-8) benefit from high FF regardless the doping concentration. This indicates that the presence of the complex  $P3HT^+ : BF_4^-$  does not have a negative impact on the FF. On the other hand, FF was significantly reduced when contact oxidation had taken place.

## 5. Conclusions

In conclusion this work shows the origin of performance parameter degradation produced by oxygen treatment of the active layer. The different effects induced by oxygen were separated by using  $NOBF_4$  as oxidant. Evidences for generation of the complex  $P3HT^+ : O_2^-$  has been shown on complete cells. This complex is responsible for photocurrent reduction. Loss in photovoltage for cells doped with molecular oxygen is in agreement with the reduced light absorption that generates less charge carriers inhibiting the Fermi level splitting (photovoltage) to some extent. On the other hand,

irreversible degradation induced by oxygen is attributed to calcium oxide formation. In this work generation of this oxide takes place only to a small degree which is responsible for a decrease in FF. These conclusions are supported by capacitance voltage measurements which provide values for degree of oxygen doping levels in the films and evidences for CaO generation.

### **Acknowledgements**

We thank financial support from Ministerio de Educacion y Ciencia under project HOPE CSD2007-00007 (Consolider-Ingenio 2010), Generalitat Valenciana under Project PROMETEO/2009/058, and Conselho Nacional de Desenvolvimento Científico e Tecnológico (CNPq) under processo 201380/2010-2.

### **Appendix A. Supplementary materials**

Supplementary data associated with this article can be found in the online version at [doi:10.1016/j.solmat.xxx](https://doi.org/10.1016/j.solmat.xxx).

## References

### Figure captions

#### Fig. 1

Representation of the current density-voltage curves of photovoltaic cells doped under different oxidant conditions: molecular oxygen (left) and NOBF<sub>4</sub> (right). \*A different metallic contact was used (LiF/Al/Ag).

#### Fig. 2

Comparison of UV-Vis spectra of P3HT in *o*-dichlorobenzene solution with the spectra of the P3HT solution after exposure to molecular oxygen (P3HT<sup>+</sup>-O<sub>2</sub><sup>-</sup>) and NOBF<sub>4</sub> (P3HT-BF<sub>4</sub><sup>-</sup>).

#### Fig. 3

Correlation between film absorption spectra (a) and EQE spectra of completed cells (b) for different oxidant conditions: molecular oxygen (left) and NOBF<sub>4</sub> (right). \*A different metallic contact was used (LiF/Al/Ag).

#### Fig. 4

Correlation between short-circuit current density and doping level. Data correspond to reference cell 1, and oxygen and NOBF<sub>4</sub> treated cells. The experimental relationship  $J_{sc} \propto n^{-0.14}$  is encountered.

#### Fig. 5

Energy diagrams of an organic semiconductor showing the effect of a variation of doping levels and presence of a dielectric interlayer (CaO): (a) un-doped semiconductor, (b) semiconductor p-type doped, (c) Semiconductor heavily p-doped and (d) Effect of CaO thickness.

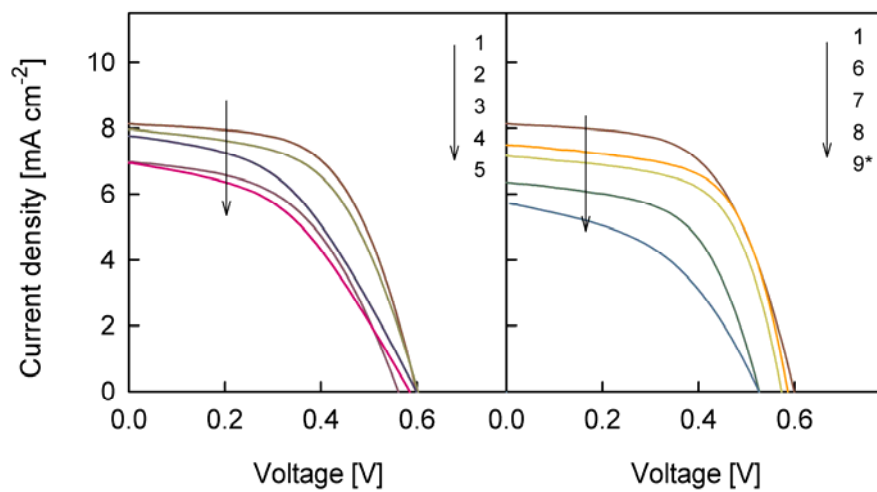


Fig. 1

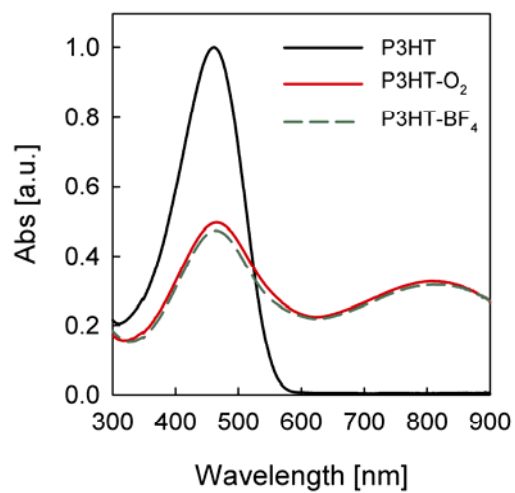


Fig. 2

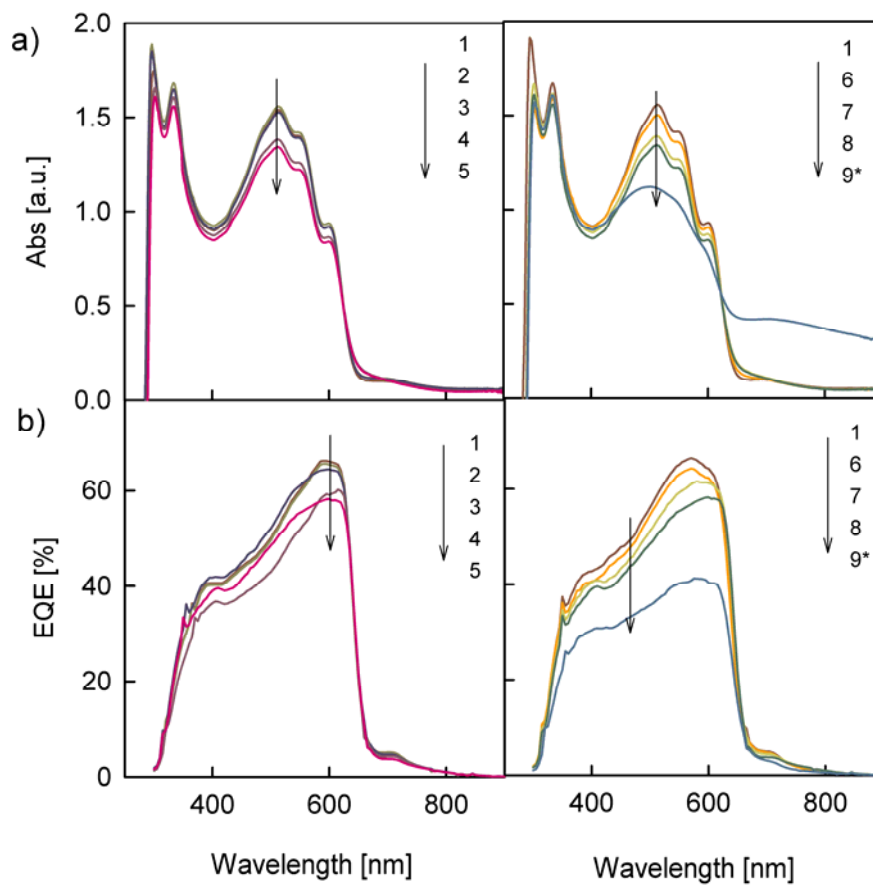


Fig. 3

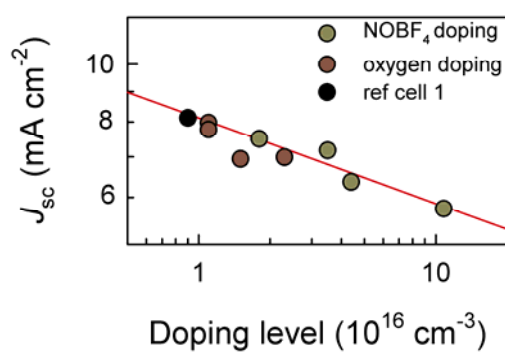


Fig. 4

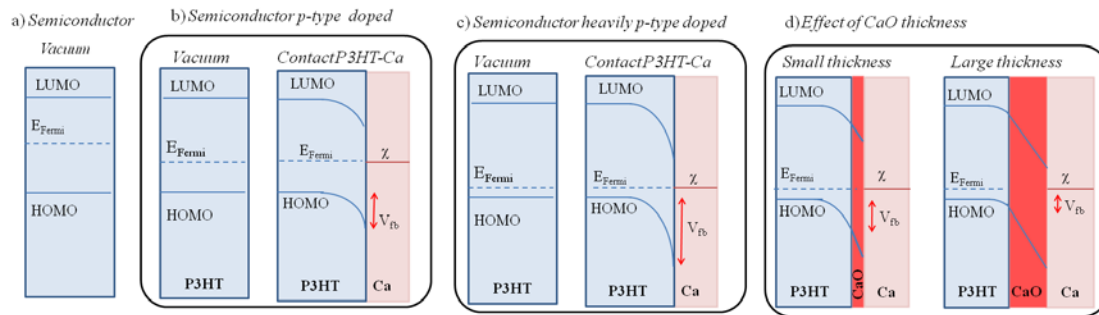
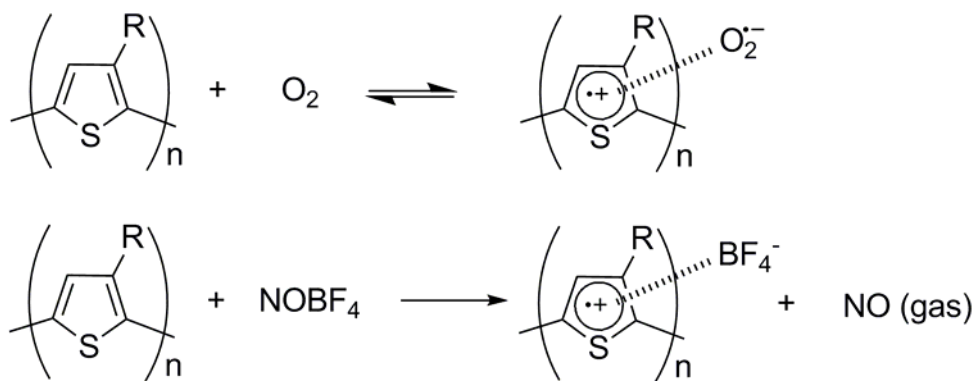


Fig. 5



**Scheme captions****Scheme 1**

Transfer complex formation of P3HT in the presence of oxygen as proposed in the literature (top) and proposed reaction of P3HT with the oxidant NOBF<sub>4</sub> (bottom).



Scheme 1

**Table captions****Table I**

Summary of preparation method and main characteristics.

<b>ID</b>	<b>Dopant</b>	<b>Method</b>	<b>Time/concentration</b>	<b>Notes</b>
1	None	---	---	Reference cell
2	O <sub>2</sub>	Flow of dry air passed through film in a chamber in the dark	2 h	Exhaustive drying step
3	O <sub>2</sub>	Flow of dry air passed through film in a chamber in the dark	1 h	
4	O <sub>2</sub>	Flow of dry air passed through film in a chamber in the dark	2 h	
5	O <sub>2</sub>	Dry air bubbled through active layer solution in the dark	10 min	
6	NOBF <sub>4</sub>	Dopant added to active layer solution	5×10 <sup>-7</sup> M	Stock solution in dichlorobenzene
7	NOBF <sub>4</sub>	Dopant added to active layer solution	1×10 <sup>-6</sup> M	Stock solution in dichlorobenzene
8	NOBF <sub>4</sub>	Dopant added to active layer solution	2×10 <sup>-6</sup> M	Stock solution in dichlorobenzene
9	NOBF <sub>4</sub>	Dopant added to active layer solution	1×10 <sup>-2</sup> M	Stock solution in acetonitrile, and LiF/Al cathode contact

**Table II**

Performance summary of solar cells with doping levels and  $V_{fb}$  extracted from  $C-V$  measurements.

<b>ID</b>	<b>Jsc</b> [mA cm <sup>-2</sup> ]	<b>Voc</b> [mV]	<b>FF</b> [%]	<b>PCE</b> [%]	<b><i>n</i></b> [x10 <sup>16</sup> cm <sup>-3</sup> ]	<b>V<sub>fb</sub></b> [mV]
1	8.13	598	58	2.8	0.9	467
2	7.98	601	55	2.6	1.1	543
3	7.77	600	45	2.1	1.1	455
4	6.94	580	45	1.8	1.5	438
5	6.99	560	50	1.9	2.3	419
6	7.50	585	62	2.7	1.8	456
7	7.17	572	61	2.5	3.5	471
8	6.36	525	57	1.9	4.4	507
9	5.74	525	45	1.4	10.8	390

## References

- [1] M.A. Green, K. Emery, Y. Hishikawa, W. Warta, Solar cell efficiency tables (version 35), *Progress in Photovoltaics*, 18 (2010) 144-150.
- [2] M. Jørgensen, K. Norrman, F.C. Krebs, Stability/degradation of polymer solar cells, *Sol. Energy Mater. Sol. Cells*, 92 (2008) 686–714.
- [3] K. Norrman, S.A. Gevorgyan, F.C. Krebs, Water-Induced Degradation of Polymer Solar Cells Studied by (H<sub>2</sub>O)-O-18 Labeling, *ACS Applied Materials & Interfaces*, 1 (2009) 102-112.
- [4] M.O. Reese, A.J. Morfa, M.S. White, N. Kopidakis, S.E. Shaheen, G. Rumbles, D.S. Ginley, Pathways for the degradation of organic photovoltaic P3HT:PCBM based devices, *Solar Energy Materials and Solar Cells*, 92 (2008) 746-752.
- [5] M. Manceau, A. Rivaton, J.L. Gardette, S. Guillerez, N. Lemaitre, The mechanism of photo- and thermooxidation of poly(3-hexylthiophene) (P3HT) reconsidered, *Polymer Degradation and Stability*, 94 (2009) 898-907.
- [6] H.J. Kim, H.H. Lee, J.J. Kim, Real Time Investigation of the Interface between a P3HT:PCBM Layer and an Al Electrode during Thermal Annealing, *Macromolecular Rapid Communications*, 30 (2009) 1269-1273.
- [7] C.F. Zhang, Y. Hao, S.W. Tong, Z.H. Lin, Q.A. Feng, E.T. Kang, C.X. Zhu, Effects of Cathode Confinement on the Performance of Polymer/Fullerene Photovoltaic Cells in the Thermal Treatment, *IEEE Transactions on Electron Devices*, 58 (2011) 835-842.
- [8] F.C. Krebs, S.A. Gevorgyan, J. Alstrup, A roll-to-roll process to flexible polymer solar cells: model studies, manufacture and operational stability studies, *Journal of Materials Chemistry*, 19 (2009) 5442-5451.
- [9] J. Schafferhans, A. Baumann, C. Deibel, V. Dyakonov, Trap distribution and the impact of oxygen-induced traps on the charge transport in poly(3-hexylthiophene), *Applied Physics Letters*, 93 (2008) 093303.
- [10] A. Tapponnier, I. Biaggio, P. Gunter, Ultrapure C-60 field-effect transistors and the effects of oxygen exposure, *Applied Physics Letters*, 86 (2005) 112114.
- [11] T. Matsushima, M. Yahiro, C. Adachi, Estimation of electron traps in carbon-60 field-effect transistors by a thermally stimulated current technique, *Applied Physics Letters*, 91 (2007) 103505.

- [12] M.T. Lloyd, D.C. Olson, P. Lu, E. Fang, D.L. Moore, M.S. White, M.O. Reese, D.S. Ginley, J.W.P. Hsu, Impact of contact evolution on the shelf life of organic solar cells, *Journal of Materials Chemistry*, 19 (2009) 7638-7642.
- [13] M.S.A. Abdou, F.P. Orfino, Y. Son, S. Holdcroft, Interaction of oxygen with conjugated polymers: Charge transfer complex formation with poly(3-alkylthiophenes), *Journal of the American Chemical Society*, 119 (1997) 4518-4524.
- [14] A. Aguirre, S.C.J. Meskers, R.A.J. Janssen, H.-J. Egelhaaf, Formation of metastable charges as a first step in photoinduced degradation in p-conjugated polymer:fullerene blends for photovoltaic applications, *Organic Electronics*, 12 (2011) 1657-1662.
- [15] M. Manceau, A. Rivaton, J.L. Gardette, Involvement of Singlet Oxygen in the Solid-State Photochemistry of P3HT, *Macromolecular Rapid Communications*, 29 (2008) 1823-1827.
- [16] H. Hintz, H.J. Egelhaaf, L. Luer, J. Hauch, H. Peisert, T. Chasse, Photodegradation of P3HT-A Systematic Study of Environmental Factors, *Chemistry of Materials*, 23 (2011) 145-154.
- [17] A. Seemann, T. Sauermann, C. Lungenschmied, O. Armbruster, S. Bauer, H.J. Egelhaaf, J. Hauch, Reversible and irreversible degradation of organic solar cell performance by oxygen, *Solar Energy*, 85 (2011) 1238-1249.
- [18] S.J. Wu, J.H. Li, Q.D. Tai, F. Yan, Investigation of High-Performance Air-Processed Poly(3-hexylthiophene)/Methanofullerene Bulk-Heterojunction Solar Cells, *Journal of Physical Chemistry C*, 114 (2010) 21873-21877.
- [19] A. Guerrero, K. Kulbaba, M. Bochmann, Alkyl zinc chlorides as new initiators for the polymerization and copolymerization of isobutene, *Macromolecular Chemistry and Physics*, 209 (2008) 1714-1720.
- [20] B.A. Mattis, P.C. Chang, V. Subramanian, Performance recovery and optimization of poly(3-hexylthiophene) transistors by thermal cycling, *Synthetic Metals*, 156 (2006) 1241-1248.
- [21] G. Li, V. Shrotriya, J.S. Huang, Y. Yao, T. Moriarty, K. Emery, Y. Yang, High-efficiency solution processable polymer photovoltaic cells by self-organization of polymer blends, *Nature Materials*, 4 (2005) 864-868.
- [22] J. Hwang, D.B. Tanner, I. Schwendeman, J.R. Reynolds, Optical properties of nondegenerate ground-state polymers: Three dioxothiophene-based conjugated polymers, *Phys. Rev. B*, 67 (2003) 115205.

- [23] F. Fabregat-Santiago, G. Garcia-Belmonte, I. Mora-Seró, J. Bisquert, Characterization of nanostructured hybrid and organic solar cells by impedance spectroscopy, *Physical Chemistry Chemical Physics*, 13 (2011) 9083–9118.
- [24] P.P. Boix, A. Guerrero, L.F. Marchesi, G. Garcia-Belmonte, J. Bisquert, Current-Voltage Characteristics of Bulk Heterojunction Organic Solar Cells: Connection Between Light and Dark Curves, *Advanced Energy Materials*, 1 (2011) 1073-1078.
- [25] J. Bisquert, G. Garcia-Belmonte, A. Munar, M. Sessolo, A. Soriano, H.J. Bolink, Band unpinning and photovoltaic model for P3HT-PCBM organic bulk heterojunctions under illumination, *Chem. Phys. Lett.*, 465 (2008) 57-62.
- [26] H. Ishii, N. Hayashi, E. Ito, Y. Washizu, K. Sugi, Y. Kimura, M. Niwano, Y. Ouchi, K. Seki, Kelvin probe study of band bending at organic semiconductor/metal interfaces: examination of Fermi level alignment, *Physica Status Solidi a-Applied Research*, 201 (2004) 1075-1094.

## Appendix A. Supplementary materials

### Oxygen doping-induced photogeneration loss in P3HT:PCBM solar cells

Antonio Guerrero<sup>1\*</sup>, Pablo P. Boix<sup>1</sup>, Luís F. Marchesi<sup>1,2</sup>, Teresa Ripolles-Sanchis<sup>1</sup>, Ernesto C. Pereira<sup>2</sup>, and Germà Garcia-Belmonte<sup>1\*</sup>

*1 Photovoltaic and Optoelectronic Devices Group, Departament de Física, Universitat Jaume I, ES-12071 Castelló, Spain*

*2 Laboratório Interdisciplinar de Electroquímica e Cerâmica (LIEC), Universidade Federal de São Carlos, São Carlos, Brazil*

#### *Active layer and dopant solutions preparation*

P3HT (Rieke Metals), PCBM (Nano-C), o-dichlorobenzene (Aldrich) and NOBF<sub>4</sub> (Aldrich) were used as received without further purification. Solutions were prepared in a glovebox under a nitrogen atmosphere. The P3HT:PCBM blend (1:1, 34 mg/ml) were dissolved using dry o-dichlorobenzene and the solution was stirred at R.T. over 24 h prior to sample fabrication. A stock solution of P3HT:PCBM blend (1:1, 34 mg/ml) saturated with dry oxygen was used for sample 5. A stock solution of dopant NOBF<sub>4</sub> was prepared by addition of solid NOBF<sub>4</sub> into a mixture containing P3HT and dry o-dichlorobenzene (34 mg/ml) for cells 6-8. After addition of the solid the mixture turned very dark and generation of a dark solid was observed. Immediately after this reaction the supernatant was added to the P3HT:PCBM mixture in separate vials to provide the different dopant concentrations. Due to the small amounts of NOBF<sub>4</sub> stock solution added the PCBM is considered in this work to be constant. It is worth noting that due to the fact that generation of the dopant is a heterogeneous reaction the supernatant concentration was calculated from absorption measurements. Cell 9 was doped with a solution of  $1 \times 10^{-2}$  M NOBF<sub>4</sub> in acetonitrile after spin coating the active layer.

#### *Device fabrication*

The polymer solar cells were fabricated with a standard sandwich structure of ITO/PEDOT:PSS/P3HT:PCBM/Ca/Ag following a previously described method.<sup>[1]</sup> The fabrication process is described here to note any experimental modification. Unless otherwise stated all manipulations were carried out under an ambient atmosphere.

Poly(3,4-ethylenedioxy thiophene):polystyrene sulfonic acid (PEDOT:PSS, CLEVIOS P AI 4083) was spin coated at 5500 rpm onto an ITO coated glass substrate (7 Ohm/sq), film thickness of ~35 nm. The substrate was heated at 100 °C for 10 min to remove traces of water trapped in the hydrophilic layer. The P3HT:PCBM blend was deposited at 900 rpm for 60 s, the substrate was introduced in a petri dish and was allowed to dry over a period of 2 h. For samples doped in solution the active layer solution was prepared as described above. The active layer thickness was about 400 nm. At this point samples were transferred into the glovebox to undertake a thermal annealing. This treatment is necessary to remove any remaining solvent and to promote oxygen desorption as described in the literature.<sup>[2]</sup> Thus, samples were heated to 150 °C for 10 min. Oxygen doping was carried out at this point for cells 2-4 as described in the discussion section. Oxygen doped samples were then taken into a glovebox equipped with a thermal evaporator. Alternatively, samples doped in solution and baseline were kept all the time in the glovebox after the thermal treatment. Evaporation was carried out at a base pressure of  $3 \times 10^{-6}$  mbar and Ca (10 nm) and Ag (120 nm) were sequentially evaporated to provide a total thickness of 130 nm to ensure reflectivity of the back contact. A LiF/Al/Ag configuration was adopted for cell 9 to avoid calcium oxidation with a thickness of 0.5/50/100 nm, respectively. Devices were encapsulated by using a pressure sensitive glue (polyisobutylene, Oppanol B 12 SFN from BASF) and a glass microscopy slide.<sup>[3]</sup> Samples were then taken out of the glovebox for device characterization.

#### *Physical Characterisation*

Thin film thicknesses were measured using a Dektak 6M Stylus Profiler. Photovoltaic cells (0.9 cm<sup>2</sup> size) were characterized by current–voltage measurements using a solar simulator (ABET Technologies Sun 2000 Solar Simulator) equipped with a 1000 W ozone-free xenon lamp and a AM 1.5G filter (Oriel). The light intensity was adjusted to 100 mW/cm<sup>2</sup> with a calibrated Si solar cell. UV/Vis data was obtained using a Cary 300 Bio Spectrophotometer. Spectra were recorded using a concentration of P3HT in ODCB of 0.05 mg/ml. Two independent solutions containing the dopants were prepared. An excess of NOBF<sub>4</sub> was added to complete a final concentration of 0.3 mg/ml. The second P3HT solution was bubbled with a dry-oxygen stream for two minutes. The voltage-capacitance measurements were carried out using a Gamry Instruments Potentiostat-Galvanostat (Reference 3000). AC oscillating amplitude was as



low as 20 mV rms to maintain the linearity of the response. Measurements were performed at 300 Hz with a 0.1 V step always in dark conditions and at room temperature. These measurements were performed with Autolab PGSTAT-30 equipped with a frequency analyzer module.

Figure A3 shows the variation of the series resistance extracted from the impedance spectroscopy analysis as a function of the applied voltage for the reference sample 1, a device doped with oxygen (cell 4) and one cell doped with  $\text{NOBF}_4$  (cell 8). For all voltages applied voltages, the cell doped with molecular oxygen exhibits increased  $R_s$  with respect to the reference cell. The maximum difference in series resistance between the cells is  $7 \Omega \text{ cm}^2$  found at low bias. This result further confirms that under the presence of molecular oxygen CaO is formed. Note that the additional series resistance is small indicating that formation of CaO only takes place to a small degree.

#### *Cell 9: Increased $\text{NOBF}_4$ Doping levels*

Cell 9 was prepared to prove that the extended film absorption observed for oxygen and  $\text{NOBF}_4$  doped samples corresponds to the charged complexes  $\text{P3HT}^+:\text{X}^-$  and to provide evidence for CaO generation. A further increased in the  $\text{P3HT}:\text{BF}_4$  concentration in the film was obtained by spin cast undoped solution of  $\text{P3HT}:\text{PCBM}$  followed by treatment of the film with  $\text{NOBF}_4$  dissolved in acetonitrile. This treatment produced an immediate change in colour of the film that indicated that the charged species have been generated. As discussed in the main text a high intensity new band forms in the 650-800 nm region. Note that for other cells prepared in this work doping levels were considerably lower and this absorption band only manifested as a small increase in the concentration in this region.

The as prepared heavily doped layer was rinsed with further acetonitrile and after cathode evaporation the calcium was severely oxidized and provided very low cell efficiency (0.006 %) with hardly any photocurrent or photovoltage. Obviously, this cell was not suitable for EQE measurements and did not represent a good comparison within the series. However, this provided a good evidence for CaO generation. Cathode oxidation was partially avoided by replacing the contact configuration from Ca/Ag to LiF/Al/Ag. The selection of this cathode is motivated by an expected increased stability of LiF towards oxidant species compared to Ca. This assumption is confirmed from results obtained for cell 9 whereby photovoltage exhibits larger values indicating cathode relative stabilization. Once again, there is a correlation between the drop in film

absorption intensity and the reduction in intensity on the EQE and photocurrent. Very interestingly, this new chemical species observed in the absorption spectra does not contribute to the final extracted current as can be observed from the EQE results.

### Figure captions

#### Fig. A1

a) Mott–Schottky plot of samples containing different oxygen doping levels. b) Mott–Schottky plot of samples containing different oxygen doping levels expansion.

#### Fig. A2

a) Mott–Schottky plot of samples containing different NOBF<sub>4</sub> doping levels. b) Mott–Schottky plot of samples containing different NOBF<sub>4</sub> doping levels expansion.

#### Fig. A3

Series resistance versus the applied voltage plot of a standard cell (1), cell doped with molecular oxygen (4) and cell doped with NOBF<sub>4</sub> (8).

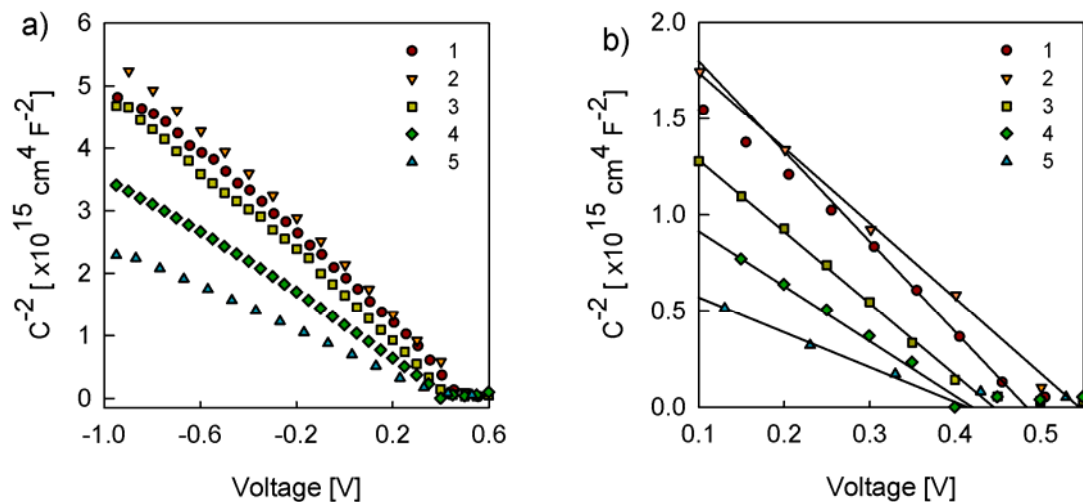


Fig. A1

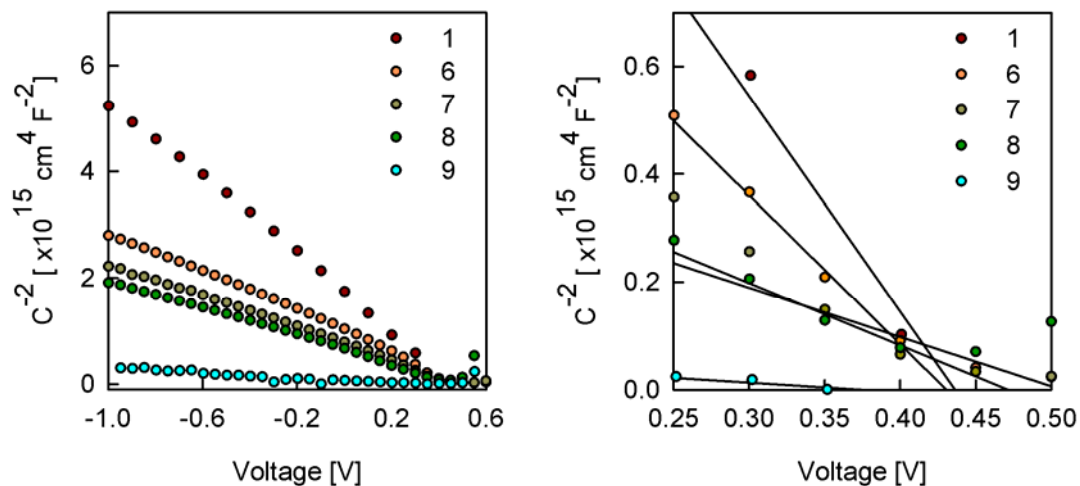


Fig. A2

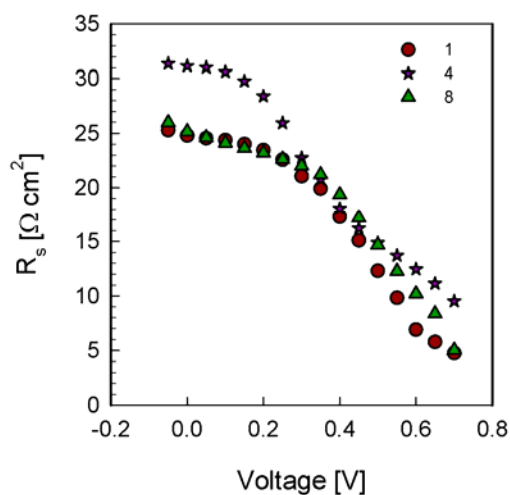


Fig. A3

[1] Y.J. He, H.Y. Chen, J.H. Hou, Y.F. Li, Indene-C-60 Bisadduct: A New Acceptor for High-Performance Polymer Solar Cells (vol 132, pg 1377, 2010), Journal of the American Chemical Society, 132 (2010) 5532-5532.

[2] S.J. Wu, J.H. Li, Q.D. Tai, F. Yan, Investigation of High-Performance Air-Processed Poly(3-hexylthiophene)/Methanofullerene Bulk-Heterojunction Solar Cells, Journal of Physical Chemistry C, 114 (2010) 21873-21877.

[3] A. Guerrero, K. Kulbaba, M. Bochmann, Alkyl zinc chlorides as new initiators for the polymerization and copolymerization of isobutene, Macromolecular Chemistry and Physics, 209 (2008) 1714-1720.

